JCTC Journal of Chemical Theory and Computation

Article

pubs.acs.org/JCTC

Analytic Calculation of Contact Densities and Mössbauer Isomer Shifts Using the Normalized Elimination of the Small-Component Formalism

Michael Filatov,*[,†] Wenli Zou,[‡] and Dieter Cremer[‡]

[†]Mulliken Center for Theoretical Chemistry, Institut für Physikalische und Theoretische Chemie, Universität Bonn, Beringstrasse 4, D-53115 Bonn, Germany

[‡]Department of Chemistry, Southern Methodist University, 3215 Daniel Avenue, Dallas, Texas 75275-0314, United States

ABSTRACT: The analytic linear response formalism for the calculation of the effective contact densities $\bar{\rho}$ in the context of the normalized elimination of the small component (NESC) method is developed and implemented. The formalism is tested for the calculation of contact densities and contact density differences in a series of mercury cations and mercury-containing molecules. The calculations carried out at the NESC/SCF, NESC/MP2, and NESC/CCSD levels of theory demonstrate high sensitivity of the contact density to the local coordination environment and the oxidation state of mercury. The NESC/MP2 results are in a very good agreement with the NESC/CCSD ones, which suggests that the former method can be used as a cost-effective alternative to high-level ab initio calculations.

1. INTRODUCTION

Mössbauer spectroscopy[1] is currently one of the most powerful analytic techniques in chemistry and physics.[2−9] It is widely used for characterization of samples rich in iron (^{57}Fe), tin (^{119}Sn), and more than 40 other elements in the periodic table, including zinc (^{67}Zn), gold (^{197}Au), mercury (^{199}Hg and ^{201}Hg), and many rare earth elements (e.g., ^{151}Eu), etc., have been investigated utilizing this technique. Besides classical Mössbauer spectroscopy, in which γ-radiation, emitted by a specific isotope nucleus, is used for the determination of the same isotope in another sample, the use of synchrotron γ-radiation in nuclear resonance scattering spectroscopy offers considerable advantages when determining resonating nuclei in very low concentrations or under extreme conditions.[10]

Mössbauer spectroscopy is based on the phenomenon of recoilless absorption of γ-radiation by the atomic nuclei embedded in a crystalline or disordered solid environment.[1] Because the frequency of the resonant γ-radiation depends on the interactions of the resonating nucleus with its electronic environment, Mössbauer spectroscopy provides information on the local electronic structure often inaccessible to other methods. Parameters of Mössbauer spectra such as the isomer shift of the nuclear γ-transition, the quadrupole splitting, and the magnetic hyperfine splitting are sensitive characteristics of the chemical environment of the resonating nucleus.

The isomer shift δ of the Mössbauer spectrum measures the difference between the energies of γ-transitions occurring in the sample (absorber) and the reference (source) nucleus. The nuclear charge radius changes during the γ-transition, and this leads to changes in the electron−nuclear interaction energy. The interpretation of the isomer shift[11−13] leads to a simple expression,

$$\delta = \alpha(\bar{\rho}^{(a)} - \bar{\rho}^{(s)}) \quad (1)$$

that relates δ (mm/s) to the so-called electron contact densities $\bar{\rho}$ at the position of the absorbing (a) and source (s) nucleus (bohr^{-3}). The calibration constant α depends on the internal parameters of the nuclear γ-transition, not all of which can be obtained experimentally or evaluated theoretically with a sufficient precision. Typically, this constant is obtained from a linear regression analysis of the theoretically calculated contact densities against the experimental values of the isomer shifts. There is a wealth of literature describing this approach, and the interested reader may be referred to a recent review, ref 9, and a recent monograph, ref 4, and references cited therein.

When calculating the contact densities, the effects of relativity and electron correlation should be appropriately taken into account. Traditionally, the contact density is obtained within the nonrelativistic formalism as electron density at the nuclear position, $\rho(0)$, and the relativistic effects not considered by the theory are absorbed by the calibration constant α.[2−4,13] This may however lead to inaccurate contact density differences and to an unreliable interpretation of the Mössbauer spectra, because, even for elements as light as ^{57}Fe, the $\rho(0)$ densities and density differences deviate from the relativistically obtained effective contact densities $\bar{\rho}$.[14] Although, for ^{57}Fe, the magnitude of relativistic effects is relatively small and the empirically obtained values of the calibration constant α are not very sensitive to the inclusion of relativity,[15,16] a good agreement with the experimentally estimated $\alpha(^{57}\text{Fe})$ was achieved in relativistically corrected ab initio calculations.[14] For heavier elements, the inclusion of relativity becomes mandatory.

An approach that enables one to straightforwardly incorporate relativistic and correlation effects into the calculated contact densities $\bar{\rho}$ was recently proposed by one of us[17] and is based on the use of linear response formalism of

Received: December 1, 2011
Published: February 2, 2012

dx.doi.org/10.1021/ct2008632 | J. Chem. Theory Comput. 2012, 8, 875−882

the isomer shift. Within this approach, the isomer shift δ (and $\overline{\rho}$) is treated as the electronic energy derivative with respect to the nuclear charge radius.[17] Initial application of this formalism[14,17−21] employed numeric differentiation of the electronic energy obtained in density functional or in high-level ab initio wave function calculations. The use of numeric differentiation is however computationally tedious and inefficient.

In the present work, a fully analytic approach to obtaining effective $\overline{\rho}$ within the linear response formalism will be presented. The method developed in the present work employs the exact two-component relativistic theory in the form of the normalized elimination of the small component (NESC) method.[22−25] The analytic energy derivatives formalism for this method has recently been developed.[26] This formalism will be adapted to the calculation of contact densities and will be applied to obtain $\overline{\rho}$ on the mercury nucleus in a series of organic and inorganic mercury compounds. A few of these compounds were recently studied by Knecht et al.[21] with a variety of theoretical methods. The current work will extend the results of previous works not only by presenting a new, more efficient and accurate formalism but also by exploring possibilities for the analytic determination of mercury in its compounds by the use of Mössbauer spectroscopy.

2. THEORY

In this section, we briefly outline the salient features of linear response theory of the Mössbauer isomer shift developed in ref 17. This formalism operates with the derivatives of the electronic energy with respect to the nuclear charge radius for obtaining the effective contact densities $\overline{\rho}$ and isomer shifts δ.

2.1. Linear Response Theory of Contact Density. The physical origin of the Mössbauer isomer shift corresponds to the variation of the nuclear charge radius during the nuclear γ-transition. Because the electron−nuclear interaction depends on the nuclear size, it will cause a slight variation of the energy of the γ-transition in the nuclei of the same isotope immersed in a different electronic environment.[2,13] The energy shift ΔE_γ of the resonance γ-transition in the a-nucleus (absorbing nucleus) with respect to the transition in the s-nucleus (source nucleus) can be sensed by Mössbauer (or nuclear γ-resonance) spectroscopy and is commonly expressed in terms of the velocity (mm/s) necessary to achieve resonance absorption due to the Doppler shift of the γ-radiation of the source nucleus; see eq 2.[2,9,13,17]

$$\delta = \frac{c}{E_\gamma}(\Delta E_\gamma^{a} - \Delta E_\gamma^{s}) \tag{2}$$

where c is the velocity of light and E_γ is the energy of the γ-quantum, $E_\gamma \gg \Delta E_\gamma^{a}, \Delta E_\gamma^{s}$. By virtue of Green's reciprocation theorem,[27] the electrons will experience exactly the same energy shift caused by the nuclear charge radius variation. Assuming (i) that a finite size nucleus is explicitly included in the calculation of the electronic energy, (ii) that the nuclear charge distribution is spherically symmetric, and (iii) that the electrons remain in the same eigenstate of the electronic Hamiltonian during the nuclear γ-transition, one can derive, to the lowest order in the variation of the charge radius ΔR_A of the nucleus A, an expression

$$\delta = \frac{c}{E_\gamma}\left(\left.\frac{\partial E^{a}(R)}{\partial R}\right|_{R=R_A} - \left.\frac{\partial E^{s}(R)}{\partial R}\right|_{R=R_A}\right)\Delta R_A \tag{3}$$

that relates the Mössbauer isomer shift to the derivatives of the electronic energy of the absorbing (E^{a}) and source (E^{s}) systems with respect to the charge radius R of the resonating nucleus.[9,17] The linear response formula 3 can be modified further by introducing the $\overline{\rho}$ which, for a given nucleus in a molecule or a crystal, is proportional to the derivative of the electronic energy with respect to the charge radius of that nucleus. By modeling the nuclear charge distribution by a Gaussian-type function[28,29] according to

$$\rho_A(r) = Z_A\left(\frac{1}{\pi\zeta^2}\right)^{3/2} e^{-r^2/\zeta^2} \tag{4}$$

the nuclear attraction potential of eq 5 is obtained:

$$V_A(r) = -\frac{Z_A}{r}\,\mathrm{erf}\left(\frac{r}{\zeta}\right) \tag{5}$$

In eq 5, r is the distance from the nucleus A, $\mathrm{erf}(x)$ is the error function, and ζ is the parameter related to the root-mean-square (rms) nuclear charge radius $\langle R^2\rangle^{1/2}$ of nucleus A as in

$$\zeta = \sqrt{\frac{2}{3}}\,\langle R^2\rangle^{1/2} \tag{6}$$

Then, the effective contact density can be obtained by[9,17]

$$\overline{\rho}_A = \frac{1}{2\pi}\frac{1}{Z_A\zeta}\left.\frac{\partial E(\zeta)}{\partial\zeta}\right|_{\zeta=\zeta_0} \tag{7}$$

in which ζ_0 is the value of the parameter obtained from the experimentally measured rms charge radius of the resonating nucleus A. The effective contact density can be directly compared to the density calculated as the expectation value of the density operator and used in connection with eq 1.[9,14,17−20] Note that in the previous works using this formalism,[9,14,17−20] eq 7 was expressed in terms of the derivatives with respect to the radius of a uniformly charged sphere $R = (5/2)^{1/2}\zeta$, which led to a different prefactor in this equation. In the following subsection, the formalism for calculating derivatives $\partial E(\zeta)/\partial\zeta$ within the context of the NESC method will be presented.

2.2. NESC Analytic Derivatives Formalism. The NESC method[22] provides the electronic (positive-energy) solutions of the Dirac equation[30] by solving the following eigenvalue equation:

$$\tilde{\mathbf{L}}\mathbf{A}_+ = \tilde{\mathbf{S}}\mathbf{A}_+\varepsilon^+ \tag{8}$$

with the relativistic metric given by

$$\tilde{\mathbf{S}} = \mathbf{S} + \frac{1}{2mc^2}\mathbf{U}^\dagger\mathbf{T}\mathbf{U} \tag{9}$$

The eigenvectors $\mathbf{A}_+$ are normalized on the metric given by eq 9 as $\mathbf{A}_+^\dagger\tilde{\mathbf{S}}\mathbf{A}_+ = \mathbf{I}$, which corresponds to the exact normalization of the large component of the relativistic four-component wave function.

dx.doi.org/10.1021/ct2008632 | J. Chem. Theory Comput. 2012, 8, 875−882

The NESC Hamiltonian $\tilde{\mathbf{L}}$ is obtained iteratively by solving the following equation:[22,24]

$$\tilde{\mathbf{L}} = \mathbf{TU} + \mathbf{U}^{\dagger}\mathbf{T} - \mathbf{U}^{\dagger}(\mathbf{T} - \mathbf{W})\mathbf{U} + \mathbf{V} \tag{10}$$

where the elimination of the small-component operator $\mathbf{U}$, which connects the large $\mathbf{A}_+$ and the pseudolarge $\mathbf{B}_+$ components of the modified Dirac wave functions via $\mathbf{B}_+ = \mathbf{UA}_+$,[22] can be obtained iteratively from[22−25,31]

$$\mathbf{U} = \mathbf{T}^{-1}(\mathbf{S}\tilde{\mathbf{S}}^{-1}\tilde{\mathbf{L}} - \mathbf{V}) \tag{11}$$

or from the solution of the modified Dirac equation.[22] The latter one-step approach was first proposed by Dyall[22] and used later by Iliaš and Saue[32] and Zou et al.[25] in practical implementations of the NESC method. The modified Dirac equation in matrix form is given by

$$\begin{pmatrix} \mathbf{V} & \mathbf{T} \\ \mathbf{T} & \mathbf{W} - \mathbf{T} \end{pmatrix}\begin{pmatrix} \mathbf{A}_- & \mathbf{A}_+ \\ \mathbf{B}_- & \mathbf{B}_+ \end{pmatrix} = \begin{pmatrix} \mathbf{S} & 0 \\ 0 & (2mc^2)^{-1}\mathbf{T} \end{pmatrix}\begin{pmatrix} \mathbf{A}_- & \mathbf{A}_+ \\ \mathbf{B}_- & \mathbf{B}_+ \end{pmatrix}\begin{pmatrix} \varepsilon^- & 0 \\ 0 & \varepsilon^+ \end{pmatrix} \tag{12}$$

where $\mathbf{A}_-$ and $\mathbf{B}_-$ are the large and the pseudolarge components of the negative-energy (positronic) states with the eigenenergies $\boldsymbol{\varepsilon}^-$ and $\mathbf{A}_+$, $\mathbf{B}_+$, and $\boldsymbol{\varepsilon}^+$ belong to the positive-energy (electronic) states.[22] With use of the solutions of eq 12, the elimination of $\mathbf{U}$ can be obtained as in

$$\mathbf{U} = \mathbf{B}_+\mathbf{A}_+^{\dagger}(\mathbf{A}_+\mathbf{A}_+^{\dagger})^{-1} = \mathbf{B}_+\mathbf{A}_+^{\dagger}\tilde{\mathbf{S}} \tag{13}$$

where $\tilde{\mathbf{S}}^{-1} = \mathbf{A}_+\mathbf{A}_+^{\dagger}$ is used.

In eqs 8−12, $\mathbf{S}$, $\mathbf{T}$, and $\mathbf{V}$ are the matrices of the overlap, kinetic energy, and potential energy operators, and $\mathbf{W}$ is the matrix of the operator $(1/4m^2c^2)\nabla V(\mathbf{r})\cdot\nabla$ in the basis of the atomic orbitals $\chi_\mu(\mathbf{r})$.[22] The scalar relativistic approximation is used throughout the paper with the velocity of light c = 137.035 999 070(98).[33]

Using the one-electron $(1e)$ approximation of Dyall,[22,34] the NESC Hamiltonian obtained in the potential field of bare nuclei is employed to obtain the energy of a many-electron system according to

$$E = tr\mathbf{PH}_{1e} + \frac{1}{2}tr\mathbf{P}(\mathbf{J} - \mathbf{K}) \tag{14}$$

for the case of the Hartree−Fock method. In eq 14, $\mathbf{J}$ and $\mathbf{K}$ are the matrices of the Coulomb and exchange operators, $\mathbf{P}$ is the usual density matrix defined as $\mathbf{P} = \mathbf{CnC}^{\dagger}$, where $\mathbf{C}$ collects the eigenvectors of the Fock operator, $\mathbf{n}$ is the diagonal matrix of the orbital occupation numbers, and $\mathbf{H}_{1e}$ is a renormalized NESC one-electron Hamiltonian as given by

$$\mathbf{H}_{1e} = \mathbf{G}^{\dagger}\tilde{\mathbf{L}}\mathbf{G} \tag{15}$$

with $\mathbf{G}$ being the renormalization matrix according to[35]

$$\mathbf{G} = \mathbf{S}^{-1/2}(\mathbf{S}^{1/2}\tilde{\mathbf{S}}^{-1}\mathbf{S}^{1/2})^{1/2}\,\mathbf{S}^{1/2} \tag{16}$$

The one-electron relativistic Hamiltonian eq 15 can be also used in connection with the Kohn−Sham energy functional or in the context of post-SCF (SCF, self-consistent field) and multireference correlated ab initio methods. For simplicity, the general formulas for the analytic energy derivatives will be formulated in the context of the Hartree−Fock method.

Differentiating eq 14 with respect to an arbitrary parameter λ (e.g., nuclear coordinates or charge radius of the nucleus), one obtains[26]

$$\frac{\partial E}{\partial\lambda} = tr\mathbf{P}\left(\frac{\partial H_{1e}}{\partial\lambda}\right) + \frac{1}{2}tr\mathbf{P}\,\frac{\partial'}{\partial\lambda}(\mathbf{J} - \mathbf{K}) - tr\boldsymbol{\Omega}\left(\frac{\partial\mathbf{S}}{\partial\lambda}\right) \tag{17}$$

where $\boldsymbol{\Omega} = \mathbf{Cn}\boldsymbol{\varepsilon}\mathbf{C}^{\dagger}$ is the energy-weighted density matrix and the prime at $\partial'/\partial\lambda$ implies that the two-electron integrals rather than the density matrix need to be differentiated.

The first term in eq 17 can be explicitly written as

$$tr\mathbf{P}\left(\frac{\partial\mathbf{H}_{1e}}{\partial\lambda}\right) = tr\mathbf{PG}^{\dagger}\frac{\partial\tilde{\mathbf{L}}}{\partial\lambda}\mathbf{G} + tr\mathbf{P}\frac{\partial\mathbf{G}^{\dagger}}{\partial\lambda}\tilde{\mathbf{L}}\mathbf{G} + tr\mathbf{PG}^{\dagger}\tilde{\mathbf{L}}\frac{\partial\mathbf{G}}{\partial\lambda} \tag{18}$$

$$= tr\tilde{\mathbf{P}}\frac{\partial\tilde{\mathbf{L}}}{\partial\lambda} + tr\mathbf{D}\frac{\partial\mathbf{G}^{\dagger}}{\partial\lambda} + tr\mathbf{D}^{\dagger}\frac{\partial\mathbf{G}}{\partial\lambda} \tag{19}$$

where new matrices $\tilde{\mathbf{P}} = \mathbf{GPG}^{\dagger}$ and $\mathbf{D} = \tilde{\mathbf{L}}\mathbf{GP}$ are introduced. Differentiating eq 10 with respect to λ and inserting the derivative into the first term of eq 18 yield

$$tr\tilde{\mathbf{P}}\frac{\partial\tilde{\mathbf{L}}}{\partial\lambda} = tr\left(\mathbf{U}\tilde{\mathbf{P}} + \tilde{\mathbf{P}}\mathbf{U}^{\dagger} - \mathbf{U}\tilde{\mathbf{P}}\mathbf{U}^{\dagger}\right)\frac{\partial\mathbf{T}}{\partial\lambda} + tr\left(\mathbf{U}\tilde{\mathbf{P}}\mathbf{U}^{\dagger}\right)\frac{\partial\mathbf{W}}{\partial\lambda} + tr\tilde{\mathbf{P}}\frac{\partial\mathbf{V}}{\partial\lambda} \tag{20}$$

$$+ tr(\mathbf{T} - (\mathbf{T} - \mathbf{W})\mathbf{U})\tilde{\mathbf{P}}\frac{\partial\mathbf{U}^{\dagger}}{\partial\lambda} + tr\tilde{\mathbf{P}}(\mathbf{T} - \mathbf{U}^{\dagger}(\mathbf{T} - \mathbf{W}))\frac{\partial\mathbf{U}}{\partial\lambda} \tag{21}$$

According to eq 30 of ref 26, the last two terms in eq 19 are given by

$$tr\left(\mathbf{D}\,\frac{\partial\mathbf{G}^{\dagger}}{\partial\lambda}\right) + tr\left(\mathbf{D}^{\dagger}\,\frac{\partial\mathbf{G}}{\partial\lambda}\right) = tr(\mathbf{D}_{0Z} + \mathbf{D}_{2Z} - \mathbf{D}_3)\,\frac{\partial\mathbf{S}}{\partial\lambda} - \frac{1}{2mc^2}\,tr(\mathbf{UD}_3\mathbf{U}^{\dagger})\,\frac{\partial\mathbf{T}}{\partial\lambda} - \frac{1}{2mc^2}\,tr\left(\mathbf{TUD}_3\,\frac{\partial\mathbf{U}^{\dagger}}{\partial\lambda} + \mathbf{D}_3\mathbf{U}^{\dagger}\mathbf{T}\,\frac{\partial\mathbf{U}}{\partial\lambda}\right) \tag{22}$$

where

$$\mathbf{D}_0 = (\mathbf{D}^{\dagger}\mathbf{G} - \mathbf{GD}^{\dagger})\mathbf{S}^{-1/2} + \mathbf{S}^{-1/2}(\mathbf{G}^{\dagger}\mathbf{D} - \mathbf{DG}^{\dagger}) \tag{23}$$

$$\mathbf{D}_1 = \mathbf{S}^{1/2}\mathbf{D}^{\dagger}\mathbf{S}^{-1/2} + \mathbf{S}^{-1/2}\mathbf{DS}^{1/2} \tag{24}$$

$$\mathbf{D}_2 = \mathbf{D}_{1Z}\mathbf{S}^{1/2}\tilde{\mathbf{S}}^{-1} + \tilde{\mathbf{S}}^{-1}\mathbf{S}^{1/2}\mathbf{D}_{1Z} \tag{25}$$

$$\mathbf{D}_3 = \tilde{\mathbf{S}}^{-1}\mathbf{S}^{1/2}\mathbf{D}_{1Z}\mathbf{S}^{1/2}\tilde{\mathbf{S}}^{-1} \tag{26}$$

and $\mathbf{D}_{0Z}$, $\mathbf{D}_{1Z}$, and $\mathbf{D}_{2Z}$ are obtained from matrices $\mathbf{D}_0$, $\mathbf{D}_1$, and $\mathbf{D}_2$ as

$$(\mathbf{D}_{qZ})_{ij} = \sum_{r,s}(\mathbf{D}_q)_{rs}\sum_{k,l}C_{ik}C_{kr}^{\dagger}C_{sl}C_{lj}^{\dagger}(m_k^{1/2} + m_l^{1/2})^{-1} \tag{27}$$

where $\mathbf{C}$ and $\mathbf{m}$ are the eigenvectors and the eigenvalues of the matrices $\mathbf{S}$ $(q = 0, 2)$ and $\mathbf{S}^{1/2}\tilde{\mathbf{S}}^{-1}\mathbf{S}^{1/2}$ $(q = 1)$ (see ref 26 for detail).

Collecting the terms in eq 19, one obtains for the gradient of the one-electron NESC energy

$$tr\mathbf{P}\left(\frac{\partial\mathbf{H}_{1e}}{\partial\lambda}\right) = tr\left(\mathbf{U}\tilde{\mathbf{P}} + \tilde{\mathbf{P}}\mathbf{U}^{\dagger} - \mathbf{U}\tilde{\mathbf{P}}\mathbf{U}^{\dagger} - \frac{1}{2mc^2}\left(\mathbf{UD}_3\mathbf{U}^{\dagger}\right)\right)\frac{\partial\mathbf{T}}{\partial\lambda} \tag{28}$$

$$+ tr\left(\mathbf{U}\tilde{\mathbf{P}}\mathbf{U}^{\dagger}\right)\frac{\partial\mathbf{W}}{\partial\lambda} + tr\tilde{\mathbf{P}}\frac{\partial\mathbf{V}}{\partial\lambda} + tr\,(\mathbf{D}_{0Z} + \mathbf{D}_{2Z} - \mathbf{D}_3)\frac{\partial\mathbf{S}}{\partial\lambda} \tag{29}$$

$$+ tr\left(\mathbf{P}_0\frac{\partial\mathbf{U}}{\partial\lambda} + \mathbf{P}_0^{\dagger}\frac{\partial\mathbf{U}^{\dagger}}{\partial\lambda}\right) \tag{30}$$

dx.doi.org/10.1021/ct2008632 | J. Chem. Theory Comput. 2012, 8, 875−882

where the matrix $\mathbf{P}_0$ is defined as

$$\mathbf{P}_0 = \tilde{\mathbf{P}}[\mathbf{T} - \mathbf{U}^\dagger(\mathbf{T} - \mathbf{W})] - \frac{1}{2mc^2}\mathbf{D}_3\mathbf{U}^\dagger\mathbf{T} \tag{31}$$

In ref 26, the derivative $\partial\mathbf{U}/\partial\lambda$ in eq 30 was obtained approximately using recurrence formulas, eqs 41 and 42 of ref 26, which provided sufficient accuracy for the geometric derivatives of the NESC total energy. In the present work, the $\partial\mathbf{U}/\partial\lambda$ derivatives are obtained exactly using the first-order response of the modified Dirac eq 12 as explained below.

Denoting the matrix operator on the left-hand side of eq 12 as $\tilde{\mathbf{D}}$, the metric matrix on the right-hand side as $\tilde{\mathbf{M}}$, the four-component wave function as $\mathbf{\Phi}$, and the matrix of the eigenvalues as $\boldsymbol{\varepsilon}$, differentiating eq 12 with respect to a perturbation λ, and multiplying the resulting equation by $\mathbf{\Phi}^\dagger$ from the left, one arrives at

$$\mathbf{O}^\lambda\boldsymbol{\varepsilon} - \boldsymbol{\varepsilon}\mathbf{O}^\lambda + \boldsymbol{\varepsilon}^\lambda = \mathbf{\Phi}^\dagger\tilde{\mathbf{D}}^\lambda\mathbf{\Phi} - \mathbf{\Phi}^\dagger\tilde{\mathbf{M}}^\lambda\mathbf{\Phi}\boldsymbol{\varepsilon} \tag{32}$$

in which the relationships $\mathbf{\Phi}^\dagger\mathbf{D}\tilde{\mathbf{\Phi}} = \boldsymbol{\varepsilon}$ and $\mathbf{\Phi}^\dagger\mathbf{M}\tilde{\mathbf{\Phi}} = \mathbf{I}$ were used, and $\boldsymbol{\varepsilon}^\lambda$, $\tilde{\mathbf{D}}^\lambda$, and $\tilde{\mathbf{M}}^\lambda$ denote the derivatives of the respective matrices with respect to the parameter λ. In eq 32, an operator $\mathbf{O}^\lambda$ is introduced, which connects the derivative of the four-component wave function with $\mathbf{\Phi}$ as in

$$\mathbf{\Phi}^\lambda = \mathbf{\Phi}\mathbf{O}^\lambda \tag{33}$$

Operator $\mathbf{O}^\lambda$ plays the central role for obtaining the derivatives $\partial\mathbf{U}/\partial\lambda$. Its matrix elements are given in

$$O_{ij}^\lambda = \begin{cases} (\varepsilon_j - \varepsilon_i)^{-1}((\mathbf{\Phi}^\dagger\tilde{\mathbf{D}}^\lambda\mathbf{\Phi})_{ij} - (\mathbf{\Phi}^\dagger\tilde{\mathbf{M}}^\lambda\mathbf{\Phi})_{ij}\varepsilon_j) & \text{for } i \neq j \\ -\frac{1}{2}(\mathbf{\Phi}^\dagger\tilde{\mathbf{M}}^\lambda\mathbf{\Phi})_{ii} & \text{for } i = j \end{cases} \tag{34}$$

Note that the diagonal elements of $\mathbf{O}^\lambda$ are obtained by differentiating the normalization condition of the four-component wave function $\mathbf{\Phi}$ and that $\mathbf{O}^\lambda$ is a nonsymmetric matrix.

Next, eq 33 is rewritten in terms of individual components of the four-component wave function $\mathbf{\Phi}$. Because we are interested in the positive-energy (electronic) states only, we will focus on the large and pseudolarge components of the electronic states.

$$\begin{pmatrix} \mathbf{A}_-^\lambda & \mathbf{A}_+^\lambda \\ \mathbf{B}_-^\lambda & \mathbf{B}_+^\lambda \end{pmatrix} = \begin{pmatrix} \mathbf{A}_- & \mathbf{A}_+ \\ \mathbf{B}_- & \mathbf{B}_+ \end{pmatrix}\begin{pmatrix} \mathbf{O}_1^\lambda & \mathbf{O}_2^\lambda \\ \mathbf{O}_3^\lambda & \mathbf{O}_4^\lambda \end{pmatrix} = \begin{pmatrix} * & \mathbf{A}_-\mathbf{O}_2^\lambda + \mathbf{A}_+\mathbf{O}_4^\lambda \\ * & \mathbf{B}_-\mathbf{O}_2^\lambda + \mathbf{B}_+\mathbf{O}_4^\lambda \end{pmatrix} \tag{35}$$

As can be seen from eq 35, response of the large and pseudolarge components of the electronic states involves mixing with the positronic states via the negative−positive block $\mathbf{O}_2^\lambda$ of the response operator $\mathbf{O}^\lambda$.

Differentiating eq 11 with respect to λ and substituting eq 35, one obtains for $\partial\mathbf{U}/\partial\lambda$

$$\frac{\partial\mathbf{U}}{\partial\lambda} = (\mathbf{B}_-\mathbf{O}_2^\lambda - \mathbf{U}\mathbf{A}_-\mathbf{O}_2^\lambda)\mathbf{A}_+^{-1} = (\mathbf{B}_-\mathbf{O}_2^\lambda - \mathbf{U}\mathbf{A}_-\mathbf{O}_2^\lambda)\mathbf{A}_+^\dagger\tilde{\mathbf{S}} \tag{36}$$

In explicit form, the $\mathbf{O}_2^\lambda$ matrix elements are given by

$$(\mathbf{O}_2^\lambda)_{ij} = (\varepsilon_j^+ - \varepsilon_i^-)^{-1}((\mathbf{\Phi}^\dagger\tilde{\mathbf{D}}_2^\lambda\mathbf{\Phi})_{ij} - (\mathbf{\Phi}^\dagger\tilde{\mathbf{M}}_2^\lambda\mathbf{\Phi})_{ij}\varepsilon_j^+) \tag{37}$$

where index i runs over positronic states, index j over electronic states, and the following negative−positive blocks of the $\tilde{\mathbf{D}}$ and $\tilde{\mathbf{M}}$ matrices are introduced

$$\mathbf{\Phi}^\dagger\tilde{\mathbf{D}}_2^\lambda\mathbf{\Phi} = \mathbf{A}_-^\dagger\frac{\partial\mathbf{V}}{\partial\lambda}\mathbf{A}_+ + \mathbf{A}_-^\dagger\frac{\partial\mathbf{T}}{\partial\lambda}\mathbf{B}_+ + \mathbf{B}_-^\dagger\frac{\partial\mathbf{T}}{\partial\lambda}\mathbf{A}_+ + \mathbf{B}_-^\dagger\left(\frac{\partial\mathbf{W}}{\partial\lambda} - \frac{\partial\mathbf{T}}{\partial\lambda}\right)\mathbf{B}_+ \tag{38}$$

$$\mathbf{\Phi}^\dagger\tilde{\mathbf{M}}_2^\lambda\mathbf{\Phi} = \mathbf{A}_-^\dagger\frac{\partial\mathbf{S}}{\partial\lambda}\mathbf{A}_+ + (2mc^2)^{-1}\mathbf{B}_-^\dagger\frac{\partial\mathbf{T}}{\partial\lambda}\mathbf{B}_+ \tag{39}$$

We now inspect eq 30, which gives the contributions of the $\partial\mathbf{U}/\partial\lambda$ operator to the NESC energy derivative. These contributions are always given by traces of matrix products,

$$\begin{aligned} tr\mathbf{P}_0\frac{\partial\mathbf{U}}{\partial\lambda} &= tr\mathbf{P}_0(\mathbf{B}_-\mathbf{O}_2^\lambda - \mathbf{U}\mathbf{A}_-\mathbf{O}_2^\lambda)\mathbf{A}_+^\dagger\tilde{\mathbf{S}} \\ &= tr\mathbf{A}_+^\dagger\tilde{\mathbf{S}}\mathbf{P}_0(\mathbf{B}_- - \mathbf{U}\mathbf{A}_-)\mathbf{O}_2^\lambda \\ &= tr\mathbf{M}'\mathbf{O}_2^\lambda \end{aligned} \tag{40}$$

which can be reformulated according to eq 40 by introducing a new matrix $\mathbf{M}' = \mathbf{A}_+^\dagger\tilde{\mathbf{S}}\mathbf{P}_0(\mathbf{B}_- - \mathbf{U}\mathbf{A}_-)$. Because the elements of the $\mathbf{O}_2^\lambda$ operator are expressed in terms of quadratic forms of the general type $\mathbf{C}_-^\dagger(\partial\mathbf{X}/\partial\lambda)\mathbf{C}_+$, where $\mathbf{C} = \mathbf{A}$, $\mathbf{B}$, and $\partial\mathbf{X}/\partial\lambda$ is a matrix of the derivatives of molecular integrals, the trace in eq 40 can be transformed as in eq 43,

$$tr\mathbf{M}'\left\{\frac{1}{\varepsilon_j^+ - \varepsilon_i^-}\left(\mathbf{C}_-^\dagger\frac{\partial\mathbf{X}}{\partial\lambda}\mathbf{C}_+\right)_{ij}\right\} = \sum_{i,j}\sum_{a,b}M'_{ji}\frac{1}{\varepsilon_j^+ - \varepsilon_i^-}(\mathbf{C}_-)_{ia}^\dagger\frac{\partial X_{ab}}{\partial\lambda}(\mathbf{C}_+)_{bj} \tag{41}$$

$$= \sum_{a,b}\left(\sum_{i,j}(\mathbf{C}_+)_{bj}M'_{ji}\frac{1}{\varepsilon_j^+ - \varepsilon_i^-}(\mathbf{C}_-)_{ia}^\dagger\right)\frac{\partial X_{ab}}{\partial\lambda} \tag{42}$$

$$= tr\mathbf{Z}\frac{\partial\mathbf{X}}{\partial\lambda} \tag{43}$$

where $\mathbf{Z}$ is a matrix with the elements given by the term in parentheses in eq 42. Thus, the contributions of the $\mathbf{U}^\lambda$ operator into the energy gradient can be conveniently formulated in terms of traces of matrix products. After some algebraic transformations, one arrives at eq 44 for the contribution of the $\partial\mathbf{U}/\partial\lambda$ derivatives to the NESC energy gradient (eq 30),

$$tr\boldsymbol{P}_0\frac{\partial\boldsymbol{U}}{\partial\lambda} = tr\boldsymbol{P}_{0V}\frac{\partial\boldsymbol{V}}{\partial\lambda} + tr\boldsymbol{P}_{0W}\frac{\partial\boldsymbol{W}}{\partial\lambda} + tr\boldsymbol{P}_{0T}\frac{\partial\boldsymbol{T}}{\partial\lambda} + tr\boldsymbol{P}_{0S}\frac{\partial\boldsymbol{S}}{\partial\lambda} \tag{44}$$

where the new matrices $\mathbf{P}_{0x}$ with $x = V, W, T, S$ are given below.

$$(\mathbf{P}_{0V})_{\nu\mu} = \sum_{i,j}(\mathbf{A}_+)_{\mu j}(\mathbf{A}_-)_{\nu i}\frac{M'_{ji}}{\varepsilon_j^+ - \varepsilon_i^-} \tag{45}$$

$$(\mathbf{P}_{0W})_{\nu\mu} = \sum_{i,j}(\mathbf{B}_+)_{\mu j}(\mathbf{B}_-)_{\nu i}\frac{M'_{ji}}{\varepsilon_j^+ - \varepsilon_i^-} \tag{46}$$

$$(\mathbf{P}_{0S})_{\nu\mu} = -\sum_{i,j}(\mathbf{A}_+)_{\mu j}(\mathbf{A}_-)_{\nu i}\frac{\varepsilon_j^+M'_{ji}}{\varepsilon_j^+ - \varepsilon_i^-} \tag{47}$$

dx.doi.org/10.1021/ct2008632 | J. Chem. Theory Comput. 2012, 8, 875−882

$$(\mathbf{P}_{0T})_{\nu\mu} = \sum_{i,j} \left\{ (\mathbf{B}_+)_{\mu j}(\mathbf{A}_-)_{\nu i} + (\mathbf{A}_+)_{\mu j}(\mathbf{B}_-)_{\nu i} - \left(1 + \frac{\varepsilon_j^+}{2mc^2}\right)(\mathbf{B}_+)_{\mu j}(\mathbf{B}_-)_{\nu i} \right\} \frac{M'_{ji}}{\varepsilon_j^+ - \varepsilon_i^-} \quad (48)$$

Thus, eqs 28−31 together with eqs 24−27 and eqs 44 and 48 complete derivation of the exact NESC analytic gradient. These equations can be used in connection with an analytic gradient geometry optimization or in connection with the first-order response formalism for obtaining various molecular properties.

Using the derivatives of molecular integrals with respect to the nuclear charge radius or with respect to the parameter ζ of the Gaussian charge distribution (4), one obtains the energy derivatives entering eq 7 for the effective contact density $\overline{\rho}_A$ at the specific nucleus A. Of all of the integral derivatives with respect to the nuclear charge radius entering eqs 28−30 and 44 only the derivatives of the electron−nuclear attraction integrals **V** and of the **W** integrals will have nonzero values. These derivatives can be easily calculated using the formalism developed by Taketa et al.[36] It is also worth noting that the application of the derivative formalism developed requires only a fraction of time needed for a single SCF iteration, because the final formulas are given in terms of traces of matrix products and scale, therefore, as N^3 with the matrix leading dimension N.

3. DETAILS OF CALCULATIONS

The formalism described in section 2 was implemented in the COLOGNE2011 suite of programs.[37] In the calculations for mercury compounds, the values of the rms nuclear charge radii of all elements were taken from compilation by Visscher and Dyall.[29] Two sets of calculations were carried out: (i) the calculations of the Hg atom and the molecules HgF, HgF_2, and HgF_4 at the NESC/SCF level using two large uncontracted basis sets; (ii) the calculations of the Hg atom and the molecules HgF, HgF_2, HgF_4, $HgCl_2$, $HgCl_4^{2-}$, $Hg(SH)_4$, $Hg(SH)_4^{2-}$, and $Hg(CH_3)_2$ at the NESC/SCF, NESC/MP2, and NESC/CCSD levels of theory using the SARC basis set[38] for mercury and the 6-31+G* basis set[39] for all other atoms. In the first set of calculations, the triple-ζ (TZ) and quadruple-ζ (QZ) basis sets of Dyall[40] in uncontracted form and modified as proposed by Knecht et al.[21] were used for Hg and the uncontracted aug-cc-pVTZ and aug-cc-pVQZ basis sets of Dunning[41] for the F atoms. In the second set of calculations, the SARC basis set for Hg was modified as follows: the two most tight primitive functions from the first s-type basis function were uncontracted and the basis set was augmented by five tight s-type primitive functions obtained in a geometric progression. The contact densities $\overline{\rho}_{Hg}$ obtained with this basis set were stable with regard to further basis set extension and closely matched the densities calculated using large uncontracted basis sets from the first set of calculations.

The molecular geometries of HgF, HgF_2, and HgF_4 were taken from ref 21, and the geometries of $HgCl_2$, $HgCl_4^{2-}$, $Hg(SH)_4$, $Hg(SH)_4^{2-}$, and $Hg(CH_3)_2$ were optimized at the NESC/MP2 level using the NESC analytic gradient technique.[26] During the NESC/MP2 geometry optimization, the 4f-, 5s-, 5p-, 5d-, and 6s-electrons of mercury and the valence electrons of other elements were correlated. When calculating the contact densities at the NESC/MP2 and NESC/CCSD levels, all electrons were correlated. The open shell species were calculated using the spin-unrestricted formalism. Atomic units of energy and density are used throughout this work.

4. RESULTS AND DISCUSSION

The formalism developed in section 2 was tested for the calculation of the derivatives $\partial E(\zeta)/\partial\zeta$, which enter eq 7. The test calculations were carried out at the NESC/SCF level for the Hg atom with the use of the TZ and QZ basis sets as described in seciton 3. The analytic derivatives $\partial E(\zeta)/\partial\zeta$ were compared with the numerically obtained derivatives. When calculating the numeric derivatives, an increment of 0.1 fm for the nuclear charge radius was used in connection with the five-point central difference formula for obtaining the first derivatives.

The results presented in Table 1 reveal that the relative deviation of the analytic derivatives from the numerically obtained ones is in the range of 10^{-6} to 10^{-7}. The analytic derivatives show a much weaker basis set dependence than the numeric ones, yielding almost the same value for the two basis sets employed. This is understandable because, in the numeric differentiation, one takes differences between very large numbers (total energies) obtained in the NESC/SCF calculations with a finite convergence criterion (a convergence criterion of 10^{-10} for the density matrix was used). In this respect, the analytic derivatives offer (besides the speed of calculation) the additional advantage of increased numeric stability.

Table 1. Comparison of the Numeric and Analytic Derivatives $\partial E(\zeta)/\partial\zeta$ (au/bohr) for the Mercury Atom[a]

	TZ	QZ
numeric	89 355.024 989	89 354.919 025
analytic, with $\partial\mathbf{U}/\partial\lambda$[b]	89 355.004 948 (2.2×10^{-7})[c]	89 355.024 006 (1.1×10^{-6})
analytic, no $\partial\mathbf{U}/\partial\lambda$[d]	89 353.262 924 (1.9×10^{-5})	89 353.282 090 (1.8×10^{-5})

[a]The derivatives are calculated at the SCF level with the use of TZ and QZ basis sets. [b]Analytic energy derivatives with the $\partial\mathbf{U}/\partial\lambda$ terms (eq 30) included. [c]Relative deviation from the numerically estimated derivative. [d]Analytic energy derivatives without the $\partial\mathbf{U}/\partial\lambda$ terms.

In the last row of Table 1, the analytic derivatives obtained when neglecting the $\partial\mathbf{U}/\partial\lambda$ terms in eq 30 are shown. Note that these terms vanish identically if one considers the electronic states completely decoupled from the positronic states (see eq 36). Surprisingly, the neglect of this coupling does not lead to a substantial deterioration of the calculated derivatives. Thus one can expect that, for properties less sensitive to the effect of relativity than the contact density (e.g., for geometric derivatives), the $\partial\mathbf{U}/\partial\lambda$ terms may be safely neglected as is confirmed by the work of Zou and co-workers.[26]

As a further test of the formalism developed, the effective contact densities of a set of mercury fluorides, HgF, HgF_2, and HgF_4, were calculated employing two large basis sets, TZ and QZ, at the NESC/SCF level of theory. The contact densities $\rho(0)$ for these compounds have been previously calculated by Knecht et al.[21] using the full four-component relativistic formalism. Note that in ref 21 the contact densities were obtained as the density values at the center of the finite size nucleus. In Table 2, the effective densities $\overline{\rho}$ obtained in this work are compared with the densities obtained by Knecht et al.[21]

dx.doi.org/10.1021/ct2008632 | J. Chem. Theory Comput. 2012, 8, 875−882

Table 2. Comparison of the Effective Contact Densities $\overline{\rho}$ (bohr^{-3}) on the Mercury Atom Obtained in This Work with the $\rho(0)$ Densities from Ref 21[a]

	TZ		QZ	
	this work	ref 21	this work	ref 21
Hg	2 104 242.499	2 363 827.39	2 104 242.948	2 363 929.12
HgF	95.957	114.54	95.946	114.48
HgF_2	117.033	127.85	116.951	127.92
HgF_4	92.393	98.09	92.347	98.09

[a]The absolute contact density is given for the Hg atom whereas for molecules the contact density differences $\overline{\rho}_{Hg} - \overline{\rho}_{mol}$ ($\rho(0)_{Hg} - \rho(0)_{mol}$ from ref 21) are listed.

The data of Table 2 reveal that $\overline{\rho}_{Hg}$ obtained with the use of the analytic formalism are less sensitive to the choice of the basis set than the $\rho(0)$ densities from ref 21. Note that $\overline{\rho}$ should not be identical to $\rho(0)$, because the latter do not include the nonuniformity of the electron distribution inside a finite-size nucleus. A difference of ca. 10% between the effective contact densities and $\rho(0)$ was already mentioned in ref 21. A similar deviation of ca. 10% was also observed for the contact density differences.[21] These observations are confirmed by the data in Table 2. As was analyzed by Knecht et al.,[21] the effect of spin−orbit interaction contributes ca. 5% to the total densities and density differences of the Hg atom and therefore does not play a significant role. These contributions are much smaller than the density differences for different compounds, and they, most likely, are not important for the interpretation of the isomer shifts in mercury compounds. Noteworthy is that general trends in the variation of the contact density differences yielded by the spin-scalar NESC formalism employed in this work are the same as those obtained in the full four-component relativistic calculations.[21]

By using a more compact SARC basis set for mercury (augmented as described in section 3), a larger set of mercury compounds was investigated. The molecules listed in Tables 3 and 4 were selected because they cover a wide range of values of the contact density varying from the value in the neutral to the doubly charged mercury atom (see Table 4).

Table 3. Molecular Geometries Used in This Work for Mercury-Containing Molecules

molecule	symmetry molecules	geometric parameter	reference
HgF	$C_{\infty v}$	r_{Hg-F} = 2.007 Å	21
HgF_2	$D_{\infty h}$	r_{Hg-F} = 1.914 Å	21
HgF_4	D_{4h}	r_{Hg-F} = 1.885 Å	21
$Hg(SH)_4$	C_{4h}	r_{Hg-S} = 2.3685 Å	
		r_{S-H} = 1.3457 Å	this work[a]
		∠HgSH = 96.4°	
$Hg(SH)_4^{2-}$	S_4	r_{Hg-S} = 2.5401 Å	
		r_{S-H} = 1.3463 Å	this work
		∠HgSH = 93.4°	
$HgCl_2$	$D_{\infty h}$	r_{Hg-Cl} = 2.2364 Å	this work
$HgCl_4^{2-}$	T_d	r_{Hg-Cl} = 2.5042 Å	this work
$Hg(CH_3)_2$	D_{3d}	r_{Hg-C} = 2.0779 Å	
		r_{S-H} = 1.0947 Å	this work
		∠HgCH = 110.4°	
$Hg(H_2O)_6^{2+}$	S_6	r_{Hg-O} = 2.3459 Å	
		r_{O-H} = 0.9792 Å	this work
		∠HgOH = 128.7°	

[a]This work: Geometries optimized using the NESC/MP2 method with the SARC basis set for mercury and 6-31+G* for all other atoms.

Molecular geometries of HgF, HgF_2, and HgF_4 were taken from ref 21. Geometries of the other molecules in Tables 3 and 4 were optimized using the NESC/MP2 method in connection with the SARC basis set[38] (augmented as described in section 3) for Hg and the 6-31+G* basis set[39] for all other atoms.

Utilizing the geometries listed in Table 3, the effective contact densities on mercury were calculated with a variety of methods. For comparison, the $\overline{\rho}$ were also calculated in mercury atomic cations, Hg^+ and Hg^{2+}, which represent the most commonly occurring oxidation states of mercury in its compounds. The contact energy differences calculated with respect to the neutral mercury atom, $\Delta\overline{\rho} = \overline{\rho}_{Hg} - \overline{\rho}_{mol}$, are listed in Table 4. The density differences account for a sufficiently wide range of values varying from ca. 40 bohr^{-3} for $Hg(CH_3)_2$ to ca. 180 bohr^{-3} for $HgCl_4^{2-}$.

From the calculated values of the density differences on the cations Hg^+ and Hg^{2+}, one might expect that $\Delta\overline{\rho}$ values of Hg-containing molecules cluster around these values for the respective oxidation states of mercury. However, the molecular $\Delta\overline{\rho}$ values are scattered across the whole range (e.g., Hg(II) in $Hg(CH_3)_2$ and $HgCl_4^{2-}$), thus revealing significant influence of the chemical environment (ligands) on the contact density. For the same type of ligands and oxidation state of mercury, there is a strong dependence on the geometry of the coordination sphere, e.g., in $HgCl_2$ and $HgCl_4^{2-}$. Thus, the contact density and the isomer shift can be used as sensitive characteristics of the local molecular structure of mercury compounds.

The results in Table 4 are presented in graphical form in Figure 1 where the contact density differences $\Delta\overline{\rho} = \overline{\rho}_{Hg} - \overline{\rho}_{mol}$ obtained using the NESC/SCF and the NESC/MP2 methods are plotted against the NESC/CCSD contact density differences. As the CCSD method is the most accurate computational scheme employed in this work, one may anticipate that (provided that all the other aspects of the molecular models chosen are correctly set up) this method is capable of yielding the contact density differences and the isomer shifts in good agreement with the experimental results. Because measured isomer shifts for Hg-containing molecules are relatively scarce, see pp 373−376 of ref 4, use of the high-level theoretical results as a reference provides a means to assess the performance of other theoretical schemes.

It is obvious from the diagrams in Figure 1 that the NESC/MP2 method performs reasonably in comparison with the considerably more expensive NESC/CCSD approach. The values of Pearson's correlation coefficient r^2 for the linear regression analysis of the NESC/SCF and NESC/MP2 results are 0.974 and 0.998, respectively. The NESC/MP2 contact density differences line up closely along the ideal correlation line (dashed line in Figure 1), whereas the NESC/SCF data are more scattered. From the NESC/SCF diagram, a group of

dx.doi.org/10.1021/ct2008632 | J. Chem. Theory Comput. 2012, 8, 875−882

Table 4. Effective Contact Densities (bohr^{-3}) on the Mercury Atom Calculated with the Use of SARC Basis Set[a]

entry[b]		NESC/SCF	NESC/MP2	NESC/CCSD
	Hg	2 104 944.971	2 105 047.821	2 105 035.382
1	Hg^{+}	112.876	127.943	121.136
2	Hg^{2+}	278.394	305.695	293.217
3	HgF	98.086	81.294	76.872
4	HgF_2	121.352	108.368	104.387
5	HgF_4	96.586	109.453	96.264
6	$Hg(SH)_4$	88.214	84.369	81.143
7	$Hg(SH)_4^{2-}$	161.635	146.332	144.369
8	$HgCl_2$	108.118	94.572	91.592
9	$HgCl_4^{2-}$	190.637	180.683	174.841
10	$Hg(CH_3)_2$	49.001	43.610	42.184
11	$Hg(H_2O)_6^{2+}$	240.820	245.550	237.066

[a]The absolute contact density is given for the mercury atom, whereas contact density differences $\bar{\rho}_{Hg} - \bar{\rho}_{mol}$ are listed for molecules. [b]Entry numbers help to identify data points in Figure 1.

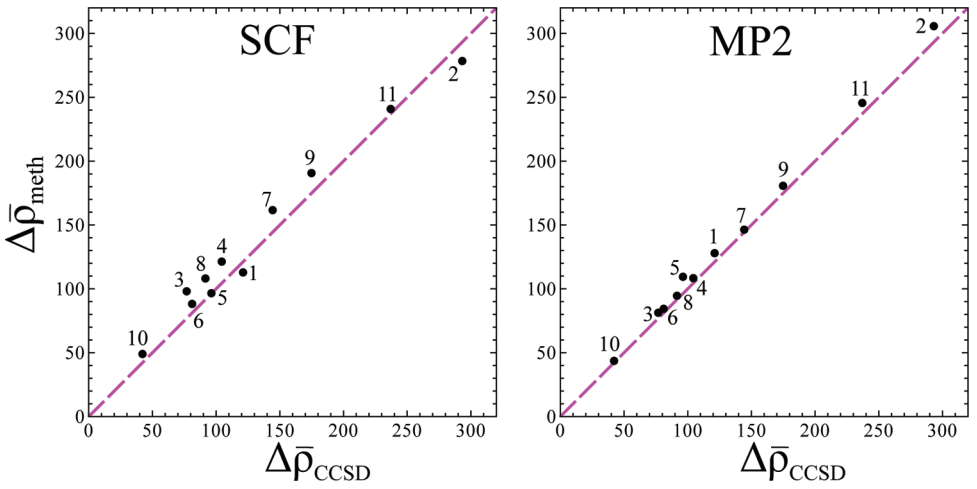

Figure 1. Contact density differences $\Delta\bar{\rho} = \bar{\rho}_{Hg} - \bar{\rho}_{mol}$ (e bohr^{-3}) calculated for mercury compounds in Table 4 using the NESC/SCF (left panel) and the NESC/MP2 (right panel) methods versus $\Delta\bar{\rho}$ calculated using the NESC/CCSD method. See Table 4 for entry numbers.

molecules containing Hg(II), $HgCl_2$ (**8**), HgF_2 (**4**), $Hg(SH)_4^{2-}$ (**7**), and $HgCl_4^{2-}$ (**9**), can be identified (the points slightly above the ideal correlation line) which show a good correlation with the NESC/CCSD results. However, the contact density differences for other compounds (and other oxidation states of Hg) follow a different trend. This implies that when parametrizing the isomer shift using eq 1 in connection with the SCF contact densities, one may need to introduce different calibration constants α for different oxidation states of mercury. A similar situation is often observed when parametrizing the isomer shift on ^{57}Fe against the contact densities from density functional calculations.[16,42] Using the contact densities from correlated methods is however free of such a deficiency, and a single calibration constant can be obtained for a specific element.[14,17,19]

In practical calculations of large molecular models, the MP2 method can be recommended as a cost-efficient alternative to the high-level CCSD method. This conclusion is in contrast to a conjecture made by Knecht et al.[21] who found that, for a limited subset of molecules in Table 4 (HgF, HgF_2, and HgF_4), MP2 did not yield a good correlation with the CCSD data. Using an extended set of molecules (as in the present work), which cover a broad range of contact density variations, helps to perform a more balanced assessment of the accuracy of various computational schemes.

5. CONCLUSIONS

In this work, the fully analytic linear response formalism of the effective contact density, eq 7, is developed in the context of the exact two-component relativistic method, the normalized elimination of the small component.[22] The formalism developed can be applied in connection with high-level wave function ab initio methods as well as with methods of density functional theory. The linear response formalism employs the one-electron approximation for the inclusion of relativistic effects,[22,34] which considerably facilitates its implementation in the existing nonrelativistic quantum chemistry codes.

The linear response formalism is tested in the calculation of the effective contact densities $\bar{\rho}$ in a series of mercury compounds. The selected molecules represent a broad range of values for the contact density, which enables one to make an unbiased judgment on the performance of the various quantum chemical computational approaches. With use of the SCF, MP2, and CCSD methods in connection with the NESC approach, it is found that (i) electron correlation plays a substantial role for the correct assessment of the changes in the contact density in dependence of the electronic environment of the Hg atom as reflected by $\Delta\bar{\rho}$, (ii) the NESC/MP2 method is capable of providing $\Delta\bar{\rho}$ values in good agreement with the NESC/CCSD method, and (iii) the contact density differences on the Hg atom are sensitive to the local chemical environment

dx.doi.org/10.1021/ct2008632 | J. Chem. Theory Comput. 2012, 8, 875−882

and to the oxidation state of Hg. The latter finding suggests that Mössbauer spectroscopy can be successfully used to characterize mercury in its molecular environment and to obtain valuable information on the electronic structure of Hg-containing molecules. We hope that this may encourage a wider use of Mössbauer spectroscopy in experimental investigation of mercury compounds.

The NESC analytic derivatives formalism, outlined in section 2, can be easily adapted to obtain other linear response properties of molecules. Substituting the appropriate molecular integral derivatives in eqs 28−30 and 44, the electric field gradient and the magnetic hyperfine structure constants can be easily calculated. Work is in progress for implementing the calculation of these parameters, which should ultimately lead to a possibility of complete and accurate theoretical characterization of the Mössbauer spectra of compounds of all the elements across the periodic table.

AUTHOR INFORMATION

Corresponding Author

*E-mail: mike.filatov@gmail.com.

Notes

The authors declare no competing financial interest.

REFERENCES

(1) Mössbauer, R. L. *Z. Phys.* **1958**, *151*, 124−143.
(2) Dunlap, B. D.; Kalvius, G. M. In *Mössbauer Isomer Shifts*; Shenoy, G. K., Wagner, F. E., Eds.; North-Holland: Amsterdam, 1978; pp 15−48.
(3) Gütlich, P.; Link, R.; Trautwein, A. *Mössbauer Spectroscopy and Transition Metal Chemistry*; Springer: Heidelberg, Germany, 1978.
(4) Gütlich, P.; Bill, E.; Trautwein, A. *Mössbauer Spectroscopy and Transition Metal Chemistry: Fundamentals and Applications*; Springer: Heidelberg, Germany, 2011.
(5) Tuček, J., Miglierini, M., Eds. *Mössbauer Spectroscopy in Materials Science;*; American Institute of Physics: College Park, MD, USA, 2010.
(6) Dyar, M. D.; Argesti, D. G.; Schaefer, M. W.; Grant, C. A.; Sklute, E. *Annu. Rev. Earth Planet. Sci.* **2006**, *34*, 83−125.
(7) Münck, E. In *Physical Methods in Bioinorganic Chemistry: Spectroscopy and Magnetism*; Que, L., Jr., Ed.; University Science Books: Sausalito, CA, USA, 2000; pp 287−320.
(8) Münck, E.; Stubna, A. In *Comprehensive Coordination Chemistry II, Vol. 2, Fundamentals: Physical Methods, Theoretical analysis and Case Studies*; McCleverty, J. A., Meyer, T. B., Lever, A. B. P., Eds.; Elsevier: New York, 2003; pp 279−286.
(9) Filatov, M. *Coord. Chem. Rev.* **2009**, *253*, 594−605.
(10) Leupold, O.; Chumakov, A. I.; Rüffer, R. In *Material Research in Atomic Scale by Mössbauer Spectroscopy*; Mashlan, M., Miglierini, M., Schaaf, P., Eds.; Kluwer Academic: Dordrecht, The Netherlands, 2003; pp 205−216.
(11) DeBenedetti, S.; Lang, G.; Ingalls, R. *Phys. Rev. Lett.* **1961**, *6*, 60−62.
(12) Walker, L. R.; Wertheim, G. K.; Jaccarino, V. *Phys. Rev. Lett.* **1961**, *6*, 98−101.
(13) Shirley, D. A. *Rev. Mod. Phys.* **1964**, *36*, 339−351.
(14) Kurian, R.; Filatov, M. *Phys. Chem. Chem. Phys.* **2010**, *12*, 2758−2762.
(15) (a) Sinnecker, S.; Slep, L. D.; Bill, E.; Neese, F. *Inorg. Chem.* **2005**, *44*, 2245−2254. (b) Römelt, M.; Ye, S.; Neese, F. *Inorg. Chem.* **2009**, *48*, 784−785.
(16) Sandala, G. M.; Hopmann, K. H.; Ghosh, A.; Noodleman, L. *J. Chem. Theory Comput.* **2011**, *7*, 3232−3247.
(17) Filatov, M. *J. Chem. Phys.* **2007**, *127*, No. 084101.
(18) Kurian, R.; Filatov, M. *J. Chem. Theory Comput.* **2008**, *4*, 278−285.
(19) Kurian, R.; Filatov, M. *J. Chem. Phys.* **2009**, *130*, No. 124121.
(20) Kurian, R.; Filatov, M. *J. Phys.: Conf. Ser.* **2010**, *217*, 012012.
(21) Knecht, S.; Fux, S.; Van Meer, R.; Visscher, L.; Reiher, M.; Saue, T. *Theor. Chem. Acc.* **2011**, *129*, 631−650.
(22) Dyall, K. G. *J. Chem. Phys.* **1997**, *106*, 9618−9626.
(23) Filatov, M. *J. Chem. Phys.* **2006**, *125*, No. 107101.
(24) Filatov, M.; Dyall, K. G. *Theor. Chem. Acc.* **2007**, *117*, 333−338.
(25) Zou, W.; Filatov, M.; Cremer, D. *Theor. Chem. Acc.* **2011**, *130*, 633−644.
(26) Zou, W.; Filatov, M.; Cremer, D. *J. Chem. Phys.* **2011**, *134*, No. 244117.
(27) Panofsky, W. K. H.; Phillips, M. *Mössbauer Spectroscopy and Transition Metal Chemistry: Fundamentals and Applications*; Addison-Wesley: Reading, MA, USA, 1962; pp 43−44.
(28) Visser, O.; Aerts, P. J. C.; Hegarty, D.; Nieuwpoort, W. C. *Chem. Phys. Lett.* **1987**, *134*, 34−38.
(29) Visscher, L.; Dyall, K. G. *At. Data Nucl. Data Tables* **1997**, *67*, 207−224.
(30) Dirac, P. A. M. *Proc. R. Soc. London* **1928**, *A117*, 610−624.
(31) Filatov, M.; Cremer, D. *J. Chem. Phys.* **2005**, *122*, No. 064104.
(32) Iliaš, M.; Saue, T. *J. Chem. Phys.* **2007**, *126*, No. 064102.
(33) Gabrielse, G.; Hanneke, D.; Kinoshita, T.; Nio, M.; Odom, B. *Phys. Rev. Lett.* **2006**, *97*, No. 030802.
(34) Dyall, K. G. *J. Comput. Chem.* **2002**, *23*, 786−793.
(35) Liu, W.; Peng, D. *J. Chem. Phys.* **2009**, *131*, No. 031104.
(36) Taketa, H.; Huzinaga, S.; O-ohata, K. *J. Phys. Soc. Jpn.* **1966**, *21*, 2313−2324.
(37) Kraka, E.; Filatov, M.; Gräfenstein, J.; Zou, W.; Joo, H.; Izotov, D.; Gauss, J.; He, Y.; Wu, A.; Polo, V.; Olsson, L.; Konkoli, Z.; He, Z.; Cremer, D. *COLOGNE2011*; Southern Methodist University: Dallas, TX, USA, 2011.
(38) Pantazis, D. A.; Chen, X.-Y.; Landis, C. R.; Neese, F. *J. Chem. Theory Comput.* **2008**, *4*, 908−919.
(39) Krishnan, R.; Binkley, J. S.; Seeger, J. A., R.; Pople. *J. Chem. Phys.* **1980**, *72*, 650−654.
(40) (a) Dyall, K. G. *Theor. Chem. Acc.* **2004**, *112*, 403−409. (b) Dyall, K. G.; Gomes, A. S. P. *Theor. Chem. Acc.* **2010**, *125*, 97−100.
(41) Dunning, T. H. Jr. *J. Chem. Phys.* **1989**, *90*, 1007−1023.
(42) Bochevarov, A. D.; Friesner, R. A.; Lippard, S. J. *J. Chem. Theory Comput.* **2010**, *6*, 3735−3749.